IOP Publishing Journal of Physics: Condensed Matter

J. Phys.: Condens. Matter **21** (2009) 263002 (19pp) doi:10.1088/0953-8984/21/26/263002

TOPICAL REVIEW

Detection of charge distributions in insulator surfaces

C A Rezende, R F Gouveia, M A da Silva and F Galembeck

Institute of Chemistry, University of Campinas—UNICAMP, PO Box 6154, CEP 13083-970, Campinas-SP, Brazil

E-mail: fernagal@iqm.unicamp.br (F Galembeck)

Received 16 March 2009, in final form 5 May 2009
Published 3 June 2009
Online at stacks.iop.org/JPhysCM/21/263002

Abstract

Charge distribution in insulators has received considerable attention but still poses great scientific challenges, largely due to a current lack of firm knowledge about the nature and speciation of charges. Recent studies using analytical microscopies have shown that insulators contain domains with excess fixed ions forming various kinds of potential distribution patterns, which are also imaged by potential mapping using scanning electric probe microscopy. Results from the authors' laboratory show that solid insulators are seldom electroneutral, as opposed to a widespread current assumption. Excess charges can derive from a host of charging mechanisms: excess local ion concentration, radiochemical and tribochemical reactions added to the partition of hydroxonium and hydronium ions derived from atmospheric water. The last factor has been largely overlooked in the literature, but recent experimental evidence suggests that it plays a decisive role in insulator charging. Progress along this line is expected to help solve problems related to unwanted electrostatic discharges, while creating new possibilities for energy storage and handling as well as new electrostatic devices.

(Some figures in this article are in colour only in the electronic version)

Contents

1. Introduction

Electrostatic phenomena have been studied for centuries and results are consolidated, for example, in Maxwell's treatise [1].

Electrical charging is present in many important technologies and processes and it is the basis for everyday applications like copying machines and laser printers [2], electrets [3, 4] that are found in a large range of equipment from acoustic transducers to gas filters [5], electrostatic painting [6], electrospinning [7] and electrostatic filtration [8].

Fundamental electrostatic concepts are well established and applications are straightforward for metals [9] and semiconductors, but not for insulators [10, 11]. In metals, induction phenomena originate from electron displacement under the action of an external electric field, forming a macroscopic electric dipole (or multipole) aligned with the field on which the solid is immersed. This reasoning is often implicitly extended to insulators, notwithstanding the slow charge displacement in these solids. Electron transfer from one insulator to another has also often been considered as the basis for contact electrification and triboelectricity.

Uncontrolled electrostatic charging may result in electrostatic accumulation and discharge, thus involving risks. Pumping low-conductivity fluids, e.g. hydrocarbons, leads to charge accumulation on the fluid that may cause fires [12] or explosions [13]. Charged dielectrics also develop cohesive adhesion forces that may interfere with polymer processing [14] and affect pharmaceutical formulations during mixing and filling [15]. Damage to electronic devices [16] is another well-known problem caused by uncontrolled electrostatic discharge. All these problems are aggravated by gaps in our understanding of electrostatic charging phenomena.

Currently, no agreement on the nature of charge carriers in electrified insulators has been achieved [10, 11, 17–22]. In the past few years, many radically new ideas on charged species and their formation mechanisms have been presented. Schein's important revision of the state of the art [10] stresses the lack of agreement on this topic. Early in 2008, McCarty and Whitesides [23] proposed that contact charging in dielectrics is largely due to partition of hydroxyl ions from water adsorbed between contacting surfaces. A few months later, Liu and Bard [24] presented evidence in favour of PTFE triboelectric charging by free electrons, upon rubbing with PMMA. There has also been great progress in the related topic of charge-transfer modelling in insulating polymers, where concepts from semiconductor physics revealed, for instance, that amorphous polyethylene has a positive electron affinity [19].

Trace numbers of charge carriers can generate measurable electric potentials and large fields adjacent to insulator surfaces. Thus, detection of the intervening species is difficult even using sophisticated current analytical techniques, and recent efforts have relied on rather complex procedures [24, 25]. Even when the charge-bearing species are not identified it is possible to estimate their excess concentrations (positive or negative) by using fundamental equations from electrostatics and the superposition principle [26]. For instance, the excess charge carrier concentration estimated for electrified paper sheets is about 1×10^{-2} unit charge μm^{-3} at 10% relative humidity, but it can produce electrostatic potential as high as 500 V [27]. This helps us to understand why the identification and speciation of charged species at insulator surfaces has been such a big challenge: because the identification of surface species present in concentrations well below 1 ppm (part per million) is required, but preferably without using photon, electron or ion beams that can produce a multitude of charged species by themselves.

Another well known but not well understood aspect of electrostatic phenomena is the importance of the surrounding atmosphere [28]. In a recent paper, Hogue *et al* highlighted the influence of atmospheric pressure on insulator–insulator contact charging and presented a model to describe the phenomenon. The authors propose a two-phase equilibrium model for surface charge based on ion transfer, which accounts for the role of atmospheric pressure and moisture layers on contact charging [29].

On the other hand, Folan *et al* did not find an effect of atmospheric water when measuring contact charging of spherical poly(styrene-divinylbenzene) copolymer particles in contact with a Ni surface. Their results indicate approximately constant charging, independent of the amount of water in the particle under ambient or a dry nitrogen atmosphere [30]. The opposite would be expected for an ion-transfer mechanism.

A recent report from Németh *et al* [31] describes the effect of water adsorption on polymer contact charging. Solvatochromic probes [32, 33] were used to characterize the Lewis acid–base properties as well as the polarity of solid surfaces [34] and the results were compared to triboelectric charging experiments under relative humidities lower than 10%. Linear correlation was found between the surface charge density and the solvatochromic data, suggesting an electron pair charge-transfer mechanism between two particles. The authors concluded [31] that the water dependent charging mechanisms overlay the fundamental charge formation process by electron pair transfer reactions. Thus, it seems that there are many relevant mechanisms for insulator charging depending on the procedure used.

1.1. Charge detection methods for insulators

Several methods for charge detection in insulators have been proposed and they can be roughly divided into methods to detect spatial distribution of charges across the materials or to map surface charges. Bulk techniques can be subdivided into a few major groups: (i) methods based on thermal diffusion [35], such as thermal pulse (TP) [36], thermal step pulse (TSP) [37] and laser intensity modulation (LIMM) [38, 39]; (ii) methods that monitor propagation of pressure waves [40], e.g. laser induced pulse pressure (LIPP) [41], pressure wave propagation (PWP) [42], piezoelectrically induced pressure step (PIPS) [43], pulsed electroacoustic (PEA) [44], non-structured acoustic pulse (NSAPM) [45] and acoustic probes [46]; and (iii) electro-optic methods based on the Pockels [47] and Kerr [48] effects.

Techniques for surface charge detection are mainly based on macroscopic or microscopic probes, such as: (i) methods based on electrostatic potential measurements, e.g. the Kelvin method [49], and (ii) microscopic methods such as Kelvin force microscopy (KFM) [50–52], electric force microscopy (EFM) [53–55] and the mirror effect in scanning electron microscopy (SEM-mirror) [56, 57].

Thermal and pressure wave methods have been used complementarily in studies of polymer electrets [58–60] and PWP was used [61] to measure charge distribution under irradiation and near-vacuum conditions [62]. Thermal-pulse tomography allowed three-dimensional imaging of space charge and polarization distributions [63], while LIMM [64] was used to obtain space charge profiles for oxides and polymer insulators used in high field applications [38, 39, 65–68].

Electro-optical methods are based on the interaction of polarized light with the electric field created by charged dielectrics. Methods based on the Pockels [47, 69] effect are mainly used on crystalline transparent solids, while those based on the Kerr effect are used for dielectric liquids [48]. Those methods can be applied to some solid materials [70] but in very special conditions.

For further information on space charge detection in dielectrics, the comprehensive review by Ahmed and Srinivas [71] is suggested.

The present work is a review of results obtained in the authors' laboratory, with a focus on the identification and speciation of charges that required an emphasis in analytical and microscopic techniques. A discussion of these techniques is presented together with unprecedented electrostatic charging phenomena. Many examples of charge distributions in insulators and the respective mechanisms for charge build-up and dissipation are also discussed.

2. Experimental methods

Our approach to the problem of charge distribution in insulators emphasized the question of the nature of the involved charges. Techniques that provide analytical information with high spatial resolution were prioritised since the initial steps of this work [72, 73], especially analytical transmission electron microscopy based on electron energy-loss spectroscopy (ESI-TEM, EELS) and scanning probe microscopy techniques (SPM), based on electric force (EFM) and potential (KFM, SEPM) measurements.

Fundamentals and a critical evaluation of these experimental methods are presented in this section.

2.1. Analytical transmission electron microscopy and elemental imaging

Electron spectroscopy imaging in the transmission electron microscope (ESI-TEM) is a technique based on electron energy loss due to inelastic scattering that allows sample elemental mapping with nanometre resolution [74–76]. When the electron beam passes through a sample, it interacts with different elements, producing all the usual effects with characteristic cross-sections. Non-scattered electrons contribute largely to the formation of bright-field images, diffracted electrons provide crystallographic information and inelastic scattering gives rise to x-rays and also to inelastically scattered electrons that are analysed using electron energy-loss spectroscopy (EELS) methods.

Inelastic electrons with different energies can be separated using different types of monochromators, as the Omega and Castaing–Henry–Ottensmeyer filters. In the latter, electrons are deflected by a prism–mirror system to different angles, so that only electrons with well-defined energies are selected at the exit slit and can be used for imaging within an analytical energy-filtered transmission electron microscope (EFTEM). Elastic scattered electrons ($\Delta E = 0$ eV) yield transmission images with reduced chromatic aberration, while monochromatic inelastic scattered electrons are used to create electron spectroscopy images (ESI). Their contrast depends on the energy-loss spectrum from the imaged area and thus on the spatial fluctuations of concentration of a particular chosen element [77, 78].

This technique has many attractive features, especially compared to competing techniques based on the analysis of x-rays produced concurrently by the electron beam [79]. First, it is very sensitive and it is even considered a 'single atom technique' [80, 81]. Furthermore, its sensitivity for light elements makes it suitable for studying many common insulators like polymers and silica films, as opposed to techniques based on x-ray spectroscopy.

It can also be used to identify nanocrystallites by plasmon imaging, but with a much higher quality than usual diffractive dark-field imaging [82].

Its main shortcoming is the inability to directly map hydrogen atoms in molecules or ions, and these have an important role in insulator charging, as shown in section 2.2. Two other limitations are common to any TEM technique: experiments are done under high vacuum, and very thin samples are required (typically about 40 nm) to avoid multiple scattering events. However, recent work from this laboratory shows that useful information can be obtained from thick samples by imaging with inelastic electrons: details of the morphology as well as chemical composition are obtained even in samples more than 100 nm thick [83].

The TEM images presented here were acquired using a Carl Zeiss CEM-902 transmission electron microscope equipped with a Castaing–Henry–Ottensmeyer energy filter spectrometer. Different setups for image acquisition were used, starting with a silicon target intensifier used in the late 1980s, upgraded to a Proscan high-speed slow-scan CCD camera, first controlled by an Analysis 3.0 system and now by an iTEM platform. At the time of writing, the acquisition of a new instrument is under way.

Sample preparation can be very simple: in the case of dispersed particles in water, a droplet of the liquid sample is deposited on carbon-coated Parlodion films supported on mesh copper grids and allowed to dry at room temperature. Solid samples have to be cut in an ultramicrotome, often under cryogenic conditions.

Image processing comprises one of the most important parts of this work. A typical procedure is given in this example [84]: a set of 38–42 images was acquired in the region of the EELS absorption edge for each element of interest, with a 6 V energy window and an energy step of 2.5 eV between the images. This set of images was used to define three energy windows used for elemental mapping. Two images were recorded at energies below the absorption threshold and used for fitting the background with a chosen function, while

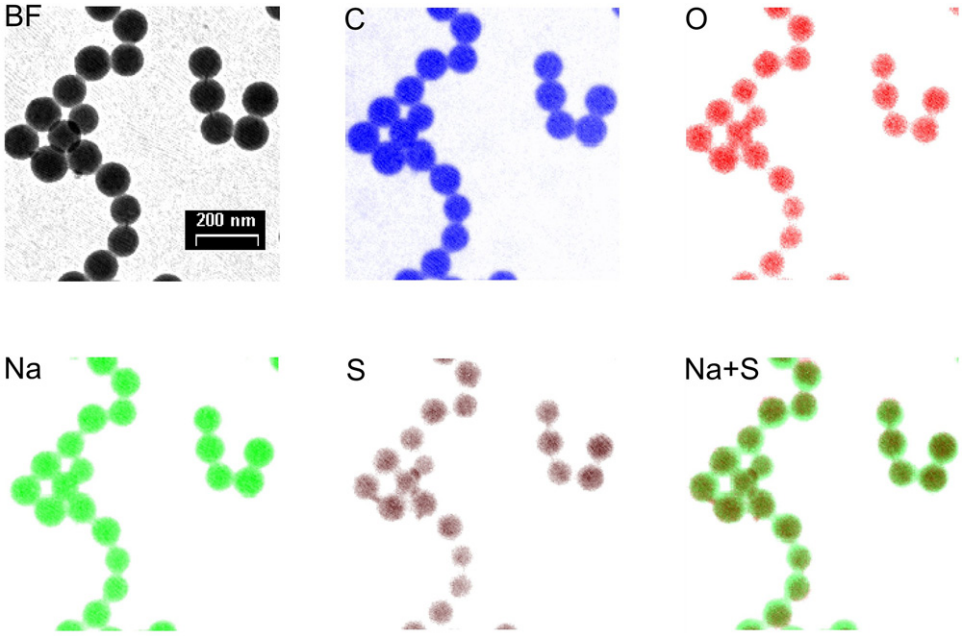

Figure 1. Bright-field (BF) micrograph of polystyrene latex particles and elemental maps of the same field, obtained by ESI-TEM for carbon (blue), oxygen (red), sodium (green) and sulfur (brown). The last picture is a superposition of the sodium and sulfur maps (Na + S).

the third image was obtained using an energy window set at the absorption band. The final elemental map image was obtained by background subtraction from the third image and it was checked for signal saturation. Each elemental map was validated by three independent checks: (i) contrast inversion in the 20–30 eV region, (ii) spectral verification, by acquisition of the energy-loss spectra, and (iii) absence of signal saturation.

Elemental images are obtained for all relevant elements found in each sample. In polymers, often-used monochromatic electrons correspond to the carbon K-edge, oxygen K-edge, sulfur L_3-edge, potassium L_3-edge and sodium L_3-edge. Brighter areas on the maps correspond to element-rich regions. Images can also be pseudo-coloured by image processing software for better visualization of the element distribution.

Representative examples of ESI-TEM micrographs are given in figure 1 for particles of polystyrene latex (PS). The use of this technique revealed that the concentration of simple ions (Na^+, K^+, RSO_4^-, Cl^- among others) shows significant spatial variations at the surface and also in the bulk of insulators. Most examined particles showed a core-and-shell structure derived from an uneven distribution of cations and anions, in contrast with the often assumed electroneutrality. These unexpected results were later confirmed by direct electrical measurements, as described in section 4.

In particular, PS latex particles show a homogeneous carbon distribution along their spherical structures, while sulfate anions (represented by oxygen and sulfur) are concentrated in the particle's inner core and cations (Na^+ and K^+) are distributed through the particle, causing charge imbalance. In the pseudo-colour images in figure 1, sodium-rich shells and sulfur-rich cores can be observed.

2.2. The Kelvin method for electrostatic potential measurements

The Kelvin method [85] is largely used for measuring electric potentials without physical contact with the sample. In 1932 this method was combined with a vibrating capacitor [86] for the development of an apparatus based on the compensation of the capacitance current between the vibrating reference electrode and the surface to be investigated [50, 87]. In a parallel-plate capacitor, the periodic displacement of a plate at a frequency ω generates current given by equation (1).

$$i(t) = V_{\mathrm{CPD}}\omega\Delta C\ \cos(\omega t) \tag{1}$$

where V_{CPD} is the potential difference between the plates and ΔC is the change in capacitance during the electrode displacement.

V_{CPD} is measured by applying a DC potential to a reference electrode oscillating over a surface, until the AC electrode current falls to zero. The DC potential applied to the vibrating reference electrode is then equal to the potential generated by fixed charges at the surface.

Great progress in the study of electrostatic patterns on insulator surfaces was achieved following the introduction of Kelvin scanning electrostatic voltmeters with various degrees of spatial resolution. These systems, based on Kelvin force microscopy (KFM) or scanning electric potential microscopy (SEPM), are especially useful since their 10 nm lateral resolution is within the macromolecular or nanoparticle size range. These will be discussed in detail in section 2.3.

The Kelvin method using macroscopic or microscopic electrodes has been used in the study of corrosion [88, 89], adsorption [90], semiconductors and metals [51, 91–96], surface contamination [97], charge pattern imaging on thin

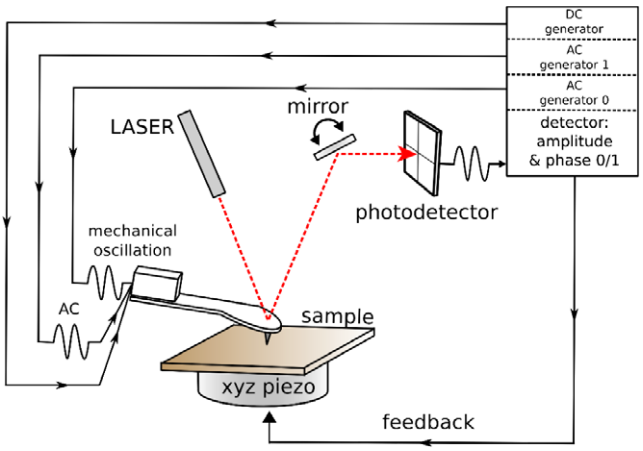

Figure 2. Schematic set-up of the scanning electric potential microscope. Adapted from [84].

film electrets [98–100] and nanopatterned surfaces [101, 102] as well as dielectric solids [103–110], thin films [111, 112], analysis of charged domains in carbon nanotubes [113] and in bioelectrochemistry for the characterization of living cells [114]. There is now growing interest in its application to a host of scientific problems.

2.3. Scanning electric potential microscopy (SEPM)/Kelvin force microscopy (KFM)

Scanning electric potential imaging is a scanning probe microscopy mode derived from non-contact AFM. It has the capability to map electrostatic potential variations on the sample surface [50, 51, 115, 116]. The technique is based on the Kelvin method, except that electrostatic forces acting on the cantilever are measured instead of AC currents [50]. The probe tip is converted into a Kelvin electrode by coating it with platinum and connecting it to DC and AC (40–70 kHz) power supplies. The DC power supply is used to bias the electrode, while the AC one introduces an alternating force component in the cantilever, which depends on the potential deriving from fixed charges of the sample. For this reason, this microscopy mode is now often known as Kelvin force microscopy (KFM). In figure 2 there is a scheme showing the basic set-up of an electric potential microscope.

The probe scans 10 nm above the sample surface and it experiences changes in the electrostatic interaction with the surface whenever the potential from the fixed charges on the sample differs from the tip potential. This interaction is nullified by varying the DC voltage applied to the tip so that the same potential is measured in both the tip and the sample [91]. The surface electric potential depends on the working functions in metals, and on the dopant concentration in semiconductors. In insulators, it depends mostly on fixed charges at the sample surface and within its bulk, including adsorption layers on the sample. The KFM or SEPM technique can thus in principle be used to obtain information on all these parameters [50].

Topography and electric potential images are simultaneously obtained. During scanning, the probe mechanical oscillation is monitored by a four-quadrant photodetector and analysed by two feedback loops. The first loop controls the tip–sample distance, while scanning the surface at constant oscillation amplitude. The AC voltage applied to keep this oscillation constant is converted into height units and used to form the topography image.

The second loop is used for surface potential measurements. A lock-in amplifier changes the DC tip bias in order to cancel the phase shift in the mechanical oscillation component of the AC signal. The DC voltage value used to zero the electric field between the tip and the sample at each pixel is converted to a grey-level or colour-coded scale to build the electric potential image.

KFM images presented in this work were obtained in a Topometrix Discoverer microscope or in a Shimadzu SPM-9600 instrument equipped with an environmental chamber.

Typical micrographs are presented in figure 3. AFM and KFM images for poly(styrene-co-hydroxyethyl methacrylate) (PS-HEMA) dry latex show significant differences: the AFM image (left) shows rather uniform packed particles with some surface protrusions, while the KFM image (right) shows that particle cores are more negative than their shells and also that there is significant variation of potential, and thus of excess charge concentration among neighbouring areas.

2.3.1. Simulation of KFM micrographs: measured electric potential distribution versus electric charge model distribution.

The electric potential created at any point adjacent to an electrostatically patterned surface can be calculated using the principle of superposition [26]. This is very useful to show how different potential patterns measured for the same fixed charge distribution depend on the probe–surface distance. A simple example is a neutral disc carrying negative charges enclosed in a ring of positive charges, as shown in figure 4. The calculation procedure was described in previous work [109].

Figure 5 presents the electric potential pattern as a function of the distance between the probe and the particle. The maps change markedly: at a distance equivalent to the probe diameter (10 nm) the potential pattern closely resembles the charge distribution, but at 100 nm the positive area looks wider and at 1 μm only negative potentials are detected. This is very intriguing, because it shows that an electroneutral object may be detected as if it were negative, at some distance. For this reason, detailed conclusions from KFM imaging can only be drawn by comparing micrographs to simulated charge distributions [109].

2.4. Electric force microscopy (EFM)

Electric force microscopy is another imaging mode that uses the conventional non-contact AFM set-up. However, it measures the electric field gradient distribution above the sample surface. A Pt-coated probe is also used, but in this case the tip is under constant bias, so that electrostatic interaction with the surface charges varies with local charge concentration. The measurement is performed in two steps: a line close to the surface (typically 10 nm) is first scanned to measure sample topography and then the same line is scanned but at about 60 nm. Topographic information is used in the second scan to track the probe at a constant height.

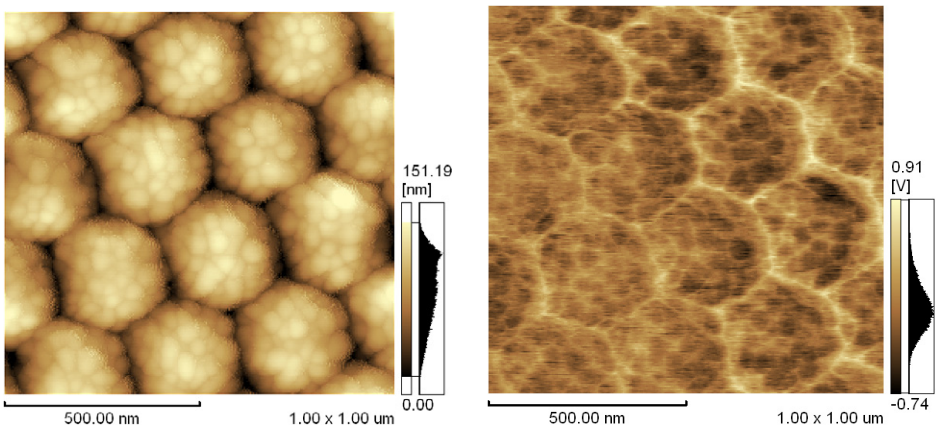

Figure 3. AFM (left) and KFM (right) images of PS-HEMA dry latex. Both images were obtained simultaneously from the same sample area.

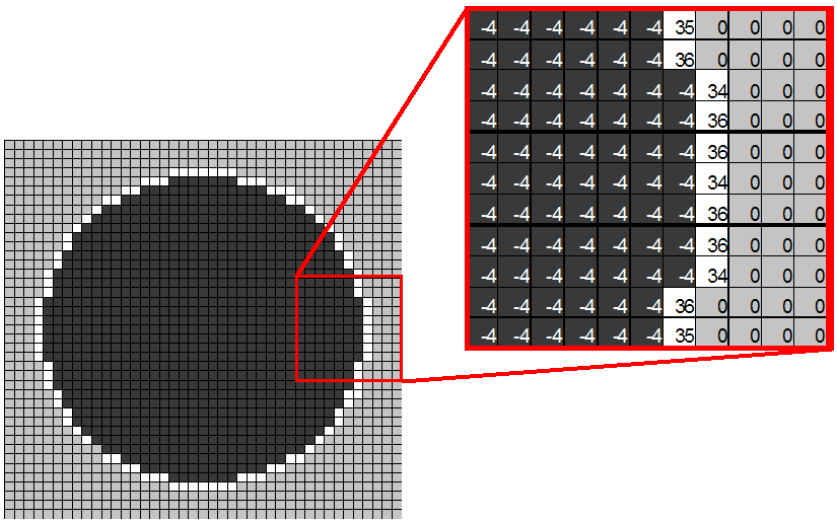

Figure 4. Model of electric charge distribution for simulating electrostatic potential measurements: the model is a neutral disc with evenly distributed negative charges enclosed within a ring of positive charges. The map is divided into 41 pixels × 41 pixels. The disc contains −4 charges per pixel (3412 total negative charges), while the ring contains 64 pixels with +36 positive charges each, 20 pixels with +35 positive charges each and 12 pixels with +34 positive charges each (3412 total positive charges), arranged symmetrically.

In the first scan, the interacting forces are dominated by short-range van der Waals interactions, while in the second one electrostatic interactions predominate, due to their lower dependence on the distance. As the tip crosses over an electrically charged region, the resonance frequency and the phase of the cantilever both change due to charge induction to the tip. The phase shift is then detected by a lock-in amplifier and used to form the electric force image.

EFM images presented here were obtained in a Topometrix Discoverer microscope using Pt-coated silicon nitride cantilevers with resonance frequency between 70 and 99 kHz and stiffness constant in the 1.8–5.2 N m^{-1} range.

2.5. Contribution of scanning probe techniques

Scanning probe techniques revealed much new and often unexpected information on electric charge distribution in insulators. Every scanned sample showed regular or complex charge patterns, and in some cases these are quite different from previous ideas. Together with potential maps acquired using macroscopic Kelvin electrodes, microscopic techniques revealed that electroneutrality is not a normal characteristic of condensed matter, at not least in the range of a few nanometres up to many centimetres, and probably in any size range considered.

In many cases, analytical TEM and scanning probe techniques were mutually validated, since excess charges and excess ion concentrations were determined independently at the same areas in a solid. However, SPM has a great advantage over TEM: images can be acquired under a large number of experimental atmospheric conditions that are inaccessible to TEM. Moreover, charge and potential detection is extremely sensitive compared to any chemical–analytical technique: excess charge concentrations as low as 10^{-10} mol l^{-1} or 10^{-5} part per million (for a 100 g mol^{-1} substance) are detected, a range out of reach of even powerful analytical techniques.

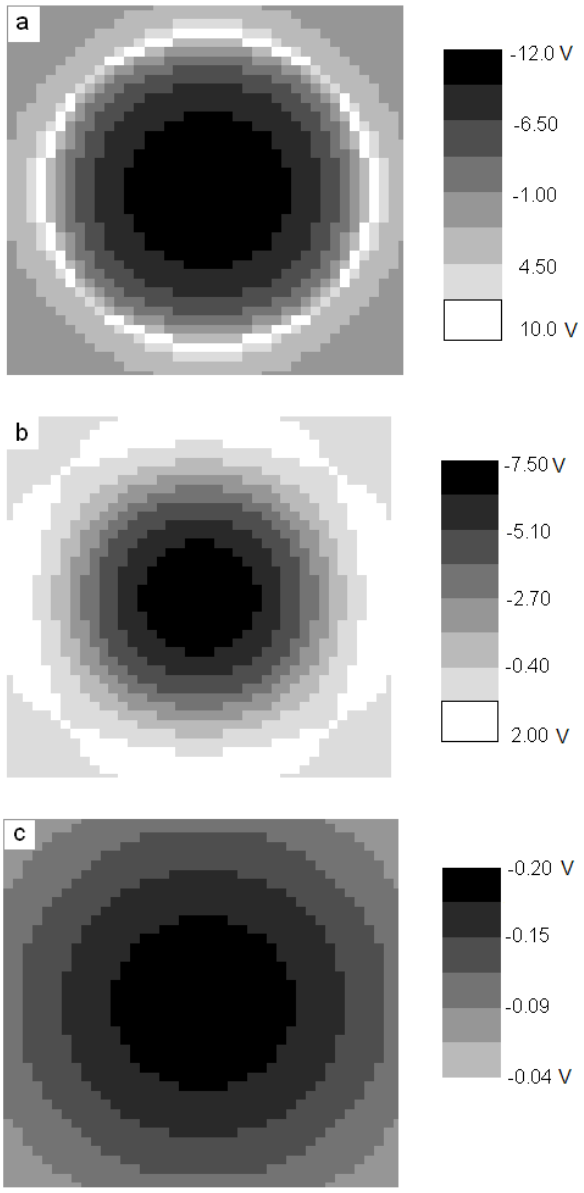

Figure 5. Electric potential maps generated by the same charge distribution on an electroneutral model particle for different distances (z-axis) between the probe and the particle: (a) 10 nm; (b)100 nm and (c) 1 μm. Particle size in the (x–y plane) is 1 × 1 μm^2.

Complex charge patterns are in turn associated with large potential gradients at insulator surfaces and in their vicinity. These can be easily calculated as the derivative of the potential profiles extracted from KFM images. For example, for the potential distribution of PS-HEMA shown in figure 3, potential profiles along two lines (line 1 and line 2, chosen in the middle upper and lower parts of the figure) are shown in figure 6 together with the calculated potential gradients in a range from −50 to +50 kV m^{-1}. Higher gradient potentials in excess of ±10 MV m^{-1} and 4 MV m^{-1} were found in Stöber silica and aluminium phosphate particles, respectively [117]. These are quite high value considering the values required for the ionization of the atmosphere and thus for the onset of electrostatic discharge [118]. This certainly has important consequences for the understanding of insulator charging, discharging and the onset of sparks in insulators.

3. Processes and mechanisms for build-up and dissipation of insulator charge

3.1. Contact between different phases and triboelectricity

Contact between metals is followed by electron transfer and interfacial charging with a polarity determined by the work functions of the contacting phases. This has also been more or less explicitly assumed as the main reason for the Maxwell effect in dielectrics, whereby contact between different phases causes charge separation at the interface. This idea was extended as far as being presented in [119, 120] as the major source for electrostatic adhesion in any solids, but the discussion on this adhesion mechanism faded many years ago [121, 122].

Triboelectricity experiments by Thales of Miletus 2500 years ago were the starting point of electrical science. The first classification of electrified bodies was also connected to mechanical behaviour, distinguishing ‘rubbery’ from ‘resinous’ electricity [123]. The relationship between contact electricity and triboelectricity is still poorly defined, since contact presumes at least mild mechanical action, but there are some efforts to distinguish these two types of charging. A complicating factor is that tribology is by itself an area with many more problems than solutions and the present authors believe that every tribology problem in insulators has an important electrostatic component.

The phase composition and, in particular, the surface composition is modified by dust particles, additives, contaminants and thin water layers, which increases the complexity of contact charging events, as characterized by Schein’s statement: ‘creating a reproducible surface and obtaining experimental reproducibility among laboratories has been a challenge’ [10].

Electrostatic charging due to contact has often been summed up in triboelectric series that were critically analysed [124] by Diaz *et al* who concluded that polymer contact charging develops from proton or ion transfer between the contacting surfaces. This idea was challenged by Liu and Bard, who found that the negative charges produced in PTFE after rubbing with PMMA are electrons [24].

However, triboelectricity extends much further than ion or electron transfer phenomena, notwithstanding the importance of these. Generation of high-energy electrons in the breaking of solids has been known for decades [125] and a dramatic example appeared recently: peeling common adhesive tape in a moderate vacuum produces radio and visible emission along with x-ray pulses that are correlated to stick–slip peeling events and can be used as a source for x-ray imaging. According to these authors [126], ‘the limits on energies and flash widths that can be achieved are beyond current theories of tribology’. This shows that the use of the ‘triboplasma’ concept developed by Heinicke [125] should be disseminated.

Friction, peeling, breaking and other mechanical actions can thus have a powerful role in producing high-energy unstable species such as ions from polyolefines and free-radicals that can further react producing ions. Vigorous

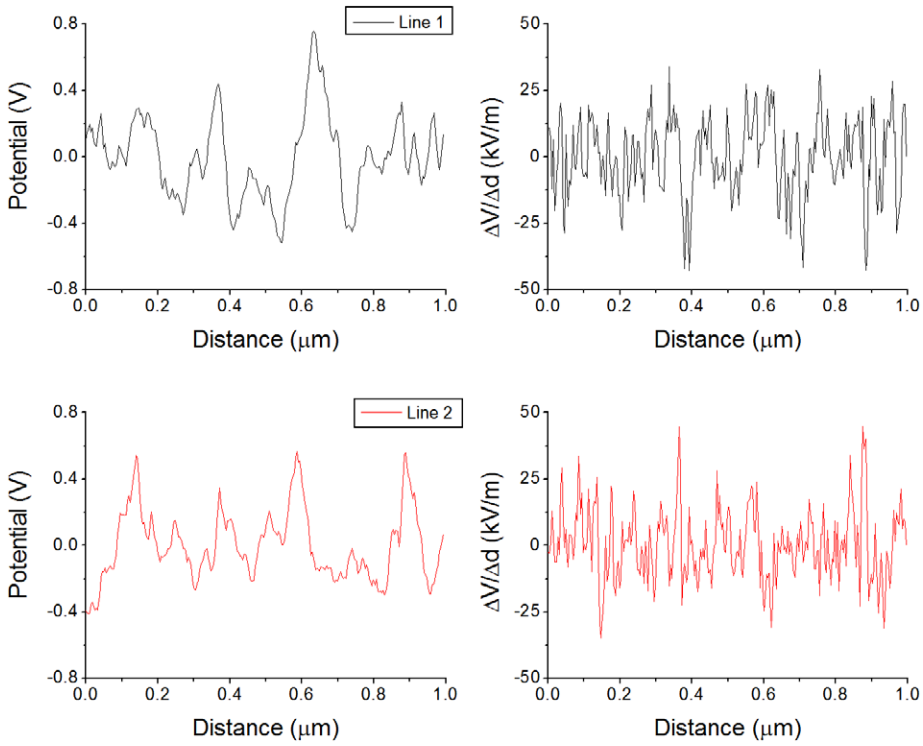

Figure 6. Potential profiles (left) along two lines extracted from the KFM image of PS-HEMA dry film in figure 5 and the respective calculated electric fields (right).

tribochemical action should thus receive the same attention as ionizing radiation in creating excess charges in otherwise stable molecular solids and liquids. Moreover, in both cases ion formation can take place within the insulating solid bulk as well as in its surface.

3.2. Ionizing radiation

The effects of ionizing radiation on macromolecules have been extensively studied [127] and they have been used for making a large number of sophisticated materials, including hybrid compounds and ceramics [128, 129].

X-rays and electron beams are used to trigger a number of reactions initiated by breaking covalent bonds and forming free-radicals and ions, that have in turn been used to make electrets [130]. It is thus not surprising that electrets are also damaged by x-rays or electron beams [131].

Das-Gupta and colleagues studied the effect of gamma radiation on the surface charge decay of corona-charged polyethylene, polypropylene and poly(ether ether ketone) (PEEK) [132, 133]. Significant differences were observed in the magnitude of charge density values for PEEK immediately after the cessation of corona charging. Irradiated polymers presented lower initial charge values than unirradiated ones, while the charge decay profile is the same.

Positive and negative ions also are produced in air, mainly due to radon and other terrestrial/cosmic radiation sources, and measuring ion concentration in air indirectly provides a measure of these sources. For this reason, electrets made out of electrically charged pieces of Teflon can be used as radiation meters, collecting ions of opposite sign. However, surprising results have been reported in the literature [134] and these may be due to the intervention of other factors in charging and discharging phenomena. In this case, ion formation can also take place both within the solid bulk and its surface.

3.3. Corona discharge and other events associated with atmospheric ionization

Corona discharge is a powerful way to produce atmospheric ions, together with light and unstable chemicals such as ozone. Corona is observed in a large number of practical situations in the laboratory or in the environment, because requirements for its onset are just a large potential gradient and some ionization mechanism (photochemical, radiochemical or other) that are fairly common. Corona discharge produces a flow of positive or negative ions that migrate through the atmosphere until they find a surface where they can bind, charging it and eventually moving to the insulator bulk. This is a convenient way to impart charge to insulators [135]. On the other hand, corona ion formation is obviously dependent on the surrounding atmosphere; consequently these ions show high variability.

Fortunately, information on atmospheric species is increasing rapidly [136], mostly due to the recent mass spectrometry sampling techniques suitable for use under normal atmosphere [137] and to new ionization devices. The positive reactant ions generated by a new source were similar to corona ions and they were identified as being solvated protons of general formula $(H_2O)_nH^+$, with $(H_2O)_2H^+$ as the most abundant species. The negative reactant ions produced were

mass identified primarily as CO_3^-, NO_3^-, NO_2^-, O_3^- and O_2^- of various relative intensities [138]. It is thus not surprising that positive and negative corona discharges may produce rather different electrification results, beyond charge signal.

At a microscopic level, new ideas on insulator charging using corona discharge through the air gap between an AFM tip and a solid surface have been presented [139, 140]. Negative and positive charges were injected into poly(methylmethacrylate) (PMMA) thin films by applying voltage pulses with an external generator to the conductive AFM tip while scanning the surface in non-contact mode. The amount of injected charge depends on the pulse intensity and on the tip–sample distance. This method allows electrostatic nanopatterning of the insulator surface, forming lasting electrets that can be used to direct nanoparticle self-assembly [140].

3.4. Ion partition

Charging by ion transfer is expected to occur by contact with a solid containing Arrhenius and Brönsted acids and bases as well as mobile counter-ions. According to this model, first proposed by Diaz *et al* [141, 142], insulators containing cations and anions with different mobilities at the surface could transfer the more mobile species to other solids, causing ion–counter-ion imbalance and surface charging when they are separated. Two important characteristics of the ion-transfer model are that the sign of charge acquired by the recipient solid after contact is always the same as the transferred ion (e.g. H^+ transferred from a carboxylate group, –COOH, will result in a positive charge in the recipient) and that the transferred ion should be detected in the recipient surface when both are separated.

This charging mechanism was observed by different authors in many systems, all involving polymers containing ionic species from molecular salts or ionomers [100, 141–147]. Diaz verified the ion-transfer model using styrene-butyl methacrylate random copolymers blended with several ionomers or molecular salts. Charges acquired by the polymer powder by contacting to ferrite beads or elastomeric surfaces agreed with the sign charge predicted by the ion-transfer model [141]. In another work, this group used x-ray photoelectron spectroscopy (XPS) to show that only the mobile ion can be detected in the other solid after contact but not the covalently bound counter-ion [145].

In the case of polystyrene doped with cetylpyridinium bromide and contacted to an indium surface, the transfer of the smaller bromide ions across the interface with the metal was observed by secondary-ion mass spectrometry (SIMS) [146]. Law *et al* studied the charging mechanism of styrene–butadiene toner particles covered with caesium 3,5-di-*tert*-butylsalicylate (CstBSA), when contacted to metal beads coated with a polymer mixture (PMMA and PVDF). This is a model system based on the xerographic developer principle. The polymeric toner particles acquired negative charge upon contacting with the polymer-coated beads, while the cation Cs^+ is uniformly detected on the bead surfaces by time-of-flight SIMS imaging (TOF-SIMS) [147].

Recent work from Whitesides and colleagues describes the use of the ion-transfer mechanism for the preparation of ionic electrets, which are materials containing unbalanced amounts of cations and anions, resulting in a long-lived electrostatic charge [23, 99, 100]. Polystyrene microspheres containing covalently bound functional groups (such as tetraalkylammonium, alkyltriphenylphosphonium, alkyl and arylsulfonate) and mobile counter-ions transfer some of their mobile groups in air upon contact and acquire a net electrostatic charge, which is consistent with the ion-transfer mechanism. The net charge on each polystyrene sphere depends on its surface area and on the dielectric constant of the surrounding gas. The charge density acquired under a SF_6 atmosphere was more than twice that under N_2.

3.5. Adsorbed water and excess charges in water

The role of water adsorbed on insulator surfaces has been acknowledged by many authors, and Schröndiger's PhD thesis was devoted to this topic [148]. It is often associated with the following factors: intrinsic water conductivity [149], its ability to dissolve surface ions and water dipole orientation in response to external electric fields. The study of adsorption layers of water on hydrophilic and hydrophobic surfaces indicates that layer thickness depends on polarization of the dispersed particles rather than the hydrophobic properties of the surface [150]. The ability of atmospheric water to trap charges was used practically in an ingenious way, creating an atmospheric plasma by trapping corona ions on fine ice particles dispersed in the air and using these to suppress electrostatic discharges while handling thermoplastic pellets [14]. More indirect evidence on the decisive role of water adsorption on electrostatic charging was given in a study on the performance of micro-electromechanical systems (MEMS) [151].

Recent work from this laboratory [109] showed reproducible electrostatic patterns on a thin film silica surface and the results were interpreted using a simple mechanism based on atmospheric water sorption–desorption coupled to charge-injection from gold electrodes into the silica film [110].

In recent years, Whitesides and collaborators proposed that contact charging in dielectrics is largely due to the partition of hydroxyl ions from water adsorbed between contacting surfaces [23]. Evidence for specific adsorption of OH^- groups at the water–air and water–oil interfaces is well established in the literature [152].

The following additional hypothesis can still be considered: electrostatic phenomena under atmospheric conditions have an important contribution from atmospheric ions [153, 154] as well as from ions generated by charging adsorbed water at the polymer surface. Atmospheric ions are charge carriers that migrate under the action of electric fields, distribute within electric potential gradients according to the Poisson–Boltzmann equation [155], adsorb on solid and liquid surfaces and discharge electrochemically on metal and semiconductor surfaces. Due to the importance of atmospheric ions for electrostatic phenomena, techniques that allow their characterization in the gas phase [156], especially under a normal atmosphere, are of particular interest [137].

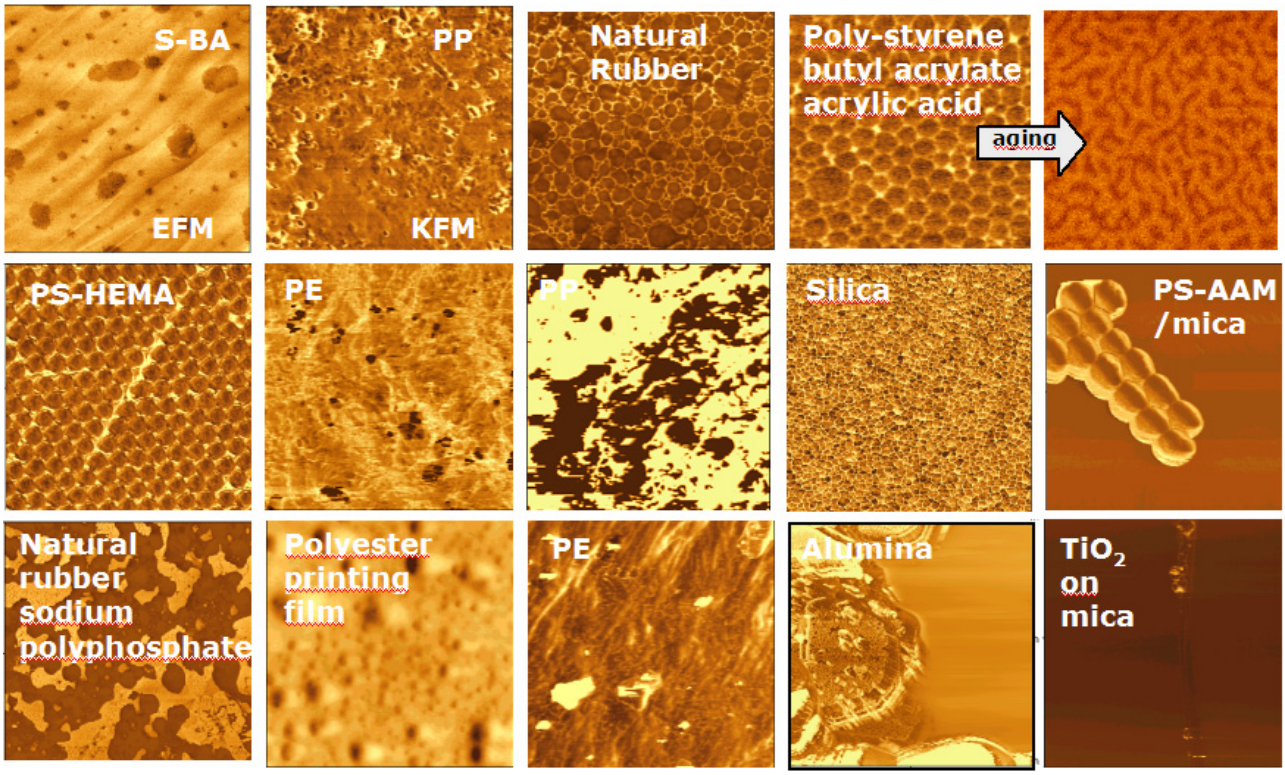

Figure 7. EFM and KFM images of some polymers and inorganic materials [106].

Moreover, adsorbed water under a given potential V acquires excess concentration of H^+ or OH^- under equilibrium, following the definition of the electrochemical potential:

$$\mu_i = \mu_i^\circ + RT \ln a_i + zFV \tag{2}$$

and the equilibrium condition, $\mu_i = \mu_i^\circ$.

Many experiments were conceived to test this hypothesis. A description of an experiment done using cellulose will be discussed in section 4. In a completely different experiment, the ability of water to store energy has been recently demonstrated [157].

3.6. Mechanisms for charge dissipation

The efforts for creating charge accumulation and transfer in insulators have not been matched by similar efforts to understand charge dissipation. The dominating idea is that charges in insulator surfaces disappear due to surface conductance, but neither the identity of the charge carrying species nor their mobilities are clear. This is further complicated by one fact: hydrophobic polymer surfaces under air in the 20–70% relative humidity range are coated with layers of water that can reach a few nanometres in thickness, on the average. However, these are hardly continuous due to dewetting events [158, 159]. A new idea is in line with section 3.5 above: charge dissipation is associated to adsorption and desorption events. In this case, a surface carrying excess negative charges, for instance, desorbs $[OH(H_2O)_n]^-$ ions and/or adsorbs $[H(H_2O)_n]^+$ ions, exchanging them with the atmosphere and thus showing a net decrease in the negative charge.

4. Electrostatic patterns in insulators

For the past ten years, many insulating materials were examined in the authors' laboratory using the techniques described in section 2 and the lesson learnt is clear: any insulator shows more or less complex charge distribution patterns. These are very stable in some cases, while in others they respond to various kinds of external stimuli or internal driving forces. In most cases, the overall solid sample charge is not equal to zero.

A set of scanning probe micrographs from polymers and some inorganic materials is shown in figure 7 to exemplify this complexity and results for some specific materials are presented in this section.

4.1. Latexes

Latexes are colloidal polymers that can be prepared from a few constituents in many different ways. The resulting particles show a large range of sizes, variable morphology and constituent distribution, which can be easily assessed by analytical TEM. Moreover, the particles are easily shaped as films or bulk solids that can be further imaged. For these reasons, latexes are very convenient for microscopy examination by various techniques, thus they were often used during this work.

Analytical TEM and KFM revealed a more or less ordered distribution of ions and electric potentials in all examined latex samples. Since the observed ions could be traced back to the compounds used in the latex synthesis and good correlation was always found between TEM and KFM images,

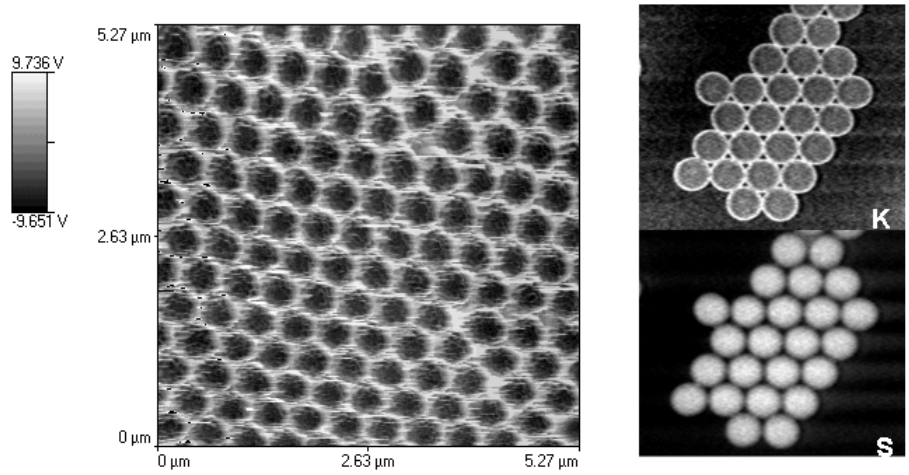

Figure 8. KFM (left) image and elemental maps obtained by ESI-TEM (right) for potassium and sulfur of a self-assembled macrocrystal of PS-HEMA latex.

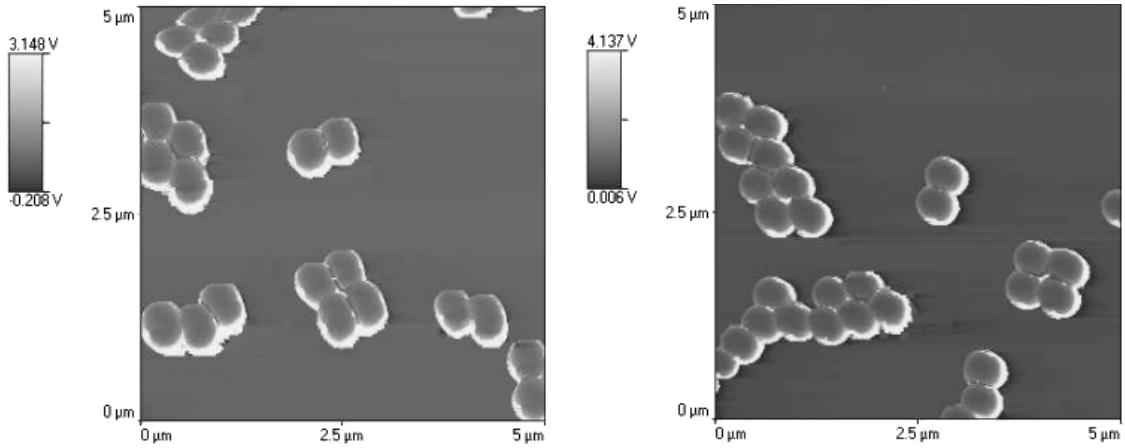

Figure 9. KFM images of PS-AAM latex acquired while scanning along two different directions. The alignment of the bright half-shell pattern is changed when the sample is rotated. Left: 0° angle and right: 45° angle.

the combination of these techniques provided new insights into latex samples, at first, and later on the distribution of charges in other insulators. A few examples follow. All the samples were analysed in their spontaneous state, no method was used for external charging of the samples.

4.1.1. Poly(styrene-co-hydroxyethyl methacrylate) (PS-HEMA) latex film. Figure 3 in section 2 presents AFM and KFM images for PS-HEMA dry latex. Latex synthesis is initiated by potassium persulfate and proceeds in aqueous emulsion in the absence of surfactant [160]. The particles in dispersion present an approximately spherical morphology but they are deformed upon drying due to capillary adhesion forces. Particle surfaces are not smooth and many protrusions can be observed. The KFM image shows a core–shell structure, with particle shells being more positive than their bulk. Each particle shows large electrical heterogeneity and the surface protrusions appear more negative than the surrounding lower surfaces. Previous analytical TEM work from this laboratory [161] showed that the negative charges result from the initiator sulfate residues attached to the polymer chains, which are spread through the inner part of the dry latex particles. On the other hand, potassium counter-ions cluster at the particle's outer layers, making a narrow shell with excess positive charge.

Potassium and sulfur maps for PS-HEMA dry latex are presented in figure 8, together with a KFM micrograph (left) of the same latex. Excellent correlation is observed between potential distribution and the location of their respective charge carrier ions.

4.1.2. Dipole formation in poly(styrene-co-acrylamide) PS-AAM latex. Figure 9 presents KFM images of poly(styrene-co-acrylamide), a latex produced by surfactant-free emulsion copolymerization of styrene (S) and acrylamide (AAM). PS-AAM latex shows a regular pattern of domains with excess electric charges: the cores are more negative (darker) than the shells, but the brighter shells always appear thicker on one side of the particles. Unexpected observations such as this must always be verified for imaging artefacts. In this experiment, image acquisition was repeated after rotating the sample 45°

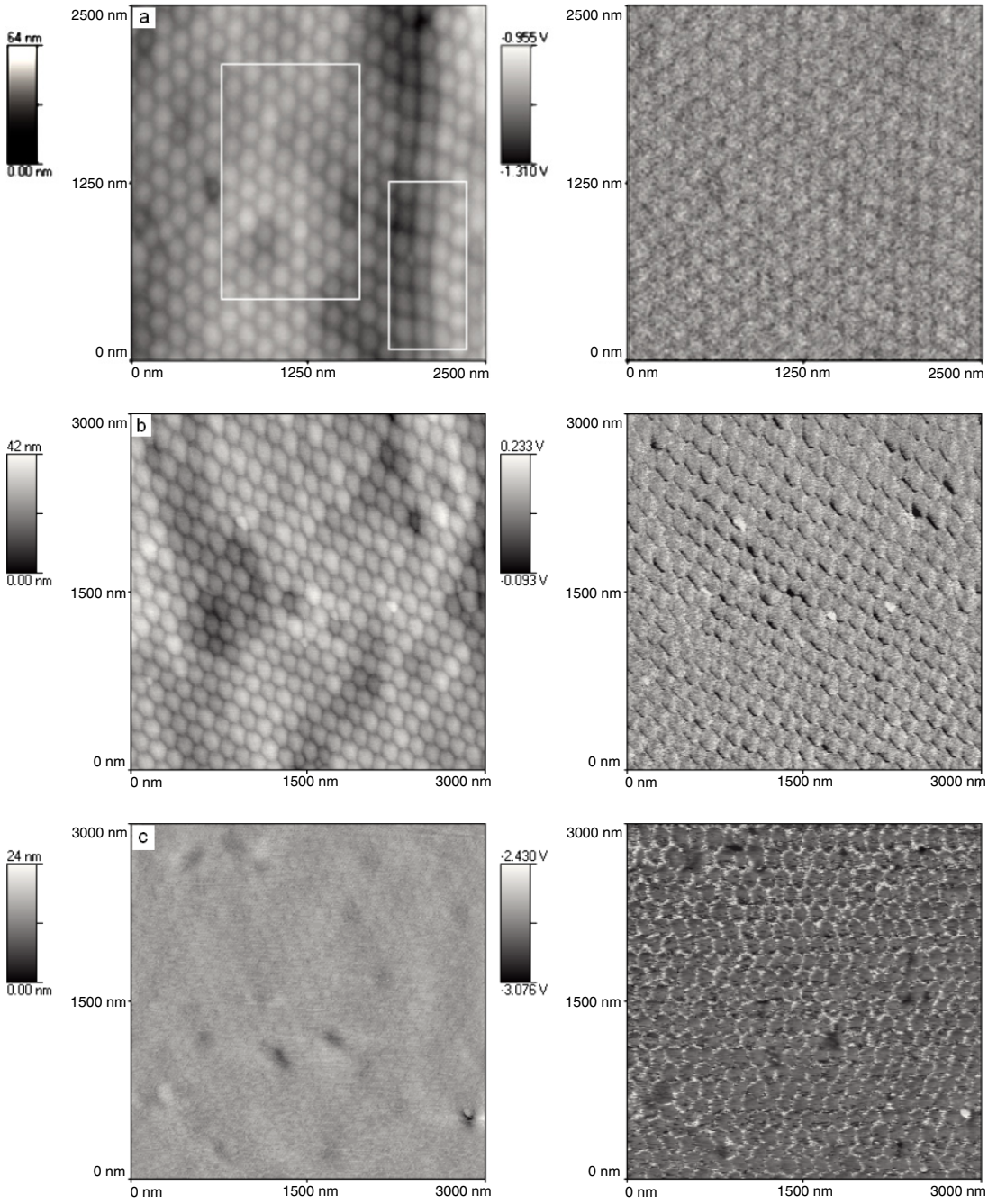

Figure 10. AFM (left) and KFM (right) images of the SB latex film on mica. (a)–(c) Images obtained on different areas of the same SB latex film.

in relation to the first scan (figure 9, right). The bright lines corresponding to positive domains also rotated for the same angle, eliminating the hypothesis of an artefact due to scanning anisotropy or tip asymmetry.

Thus, a particle dried over the mica forms a dipole, and this is aligned with the substrate crystallographic axis [162]. This behaviour was explained considering that: (i) latex particles are plastic electric multipoles or dipoles and (ii) the mica surface is anisotropic.

4.1.3. Heterogeneity in styrene–butadiene (SB) latex films. Styrene–butadiene latex is also obtained by emulsion polymerization. Figure 10 shows AFM and KFM images for different areas of the SB latex film [163]. Electric potential patterns analysed in this work are highly variable, showing a large degree of particle heterogeneity. A number of interesting observations are made: the AFM micrograph in figure 10(a) shows deformed particles packed in hexagonal (left rectangle) or cubic arrays (right rectangle). The KFM image presents a faint contrast analogous to AFM contrast but sprinkled with negative spots. Another region of the film (AFM image in figure 10(b)) shows deformed hexagons with marked electric polarization in the KFM image. Finally, figure 10(c) presents AFM and KFM images from a third film area. The

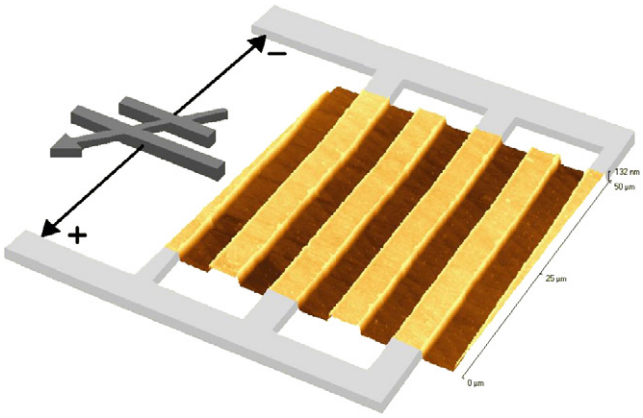

Figure 11. Illustration of the sample mounting drawn over an AFM image. Clear areas are coated with gold while dark areas are bare silica. External wiring is connected to the bus gold stripes at both sides of the figure. One electrode set is always grounded and the other is biased, positive or negative [110].

surface topography is very smooth and particle borders are not completely discernible in the AFM image. On the other hand, they are easily perceived in the KFM micrograph, where the interparticle spaces are more positive than the particle core areas. These results show a large heterogeneity within these particles. Latex films were analysed by other microscopy techniques showing that the particles are heterogeneous due to microchemical differences within their domains.

4.2. Silica-on-wafer thin film

The usual calibration sample for KFM is a thin silica film (grown by oxidation of a silicon wafer surface), partially covered with thin stripes of gold. When these are connected to a DC power supply, they form an array of alternating interdigitated electrodes, as shown in figure 11.

When the electrodes are polarized and then short-circuited, KFM imaging reveals the formation and dissipation of electrostatic patterns on silica. These are strongly dependent on the relative humidity (RH) and temperature, under an argon atmosphere (figure 12).

Figure 12 is a potential pattern representation in both space and in time. Following the image from top to bottom, many changes are observed with time, in consecutive micrographs as well as within any micrographs recorded at 70% or 50% RH values. When the electrodes are polarized under 50% RH, the initial patterns show little or no observable changes. However, the image recorded at 70% RH shows that the electric pattern changes gradually with time.

When the electrodes are all grounded, consecutive micrographs recorded at 70% RH show pronounced variations, while those recorded at lower humidity are very stable.

Electrostatic charging and discharging are thus much faster at high relative humidity, showing that the charged or discharged silica states both change faster under high humidity. On the other hand, pattern preservation is more effective under low humidity. Charge dissipation under high humidity is well known and it is often assigned to increased surface conductance. However, increased charge accumulation at high humidity is not expected within any models for surface charge accumulation, except those based in water ion partitioning [109, 110].

This results are explained using a model that considers the existence of atmospheric water and thus of ions formed by water dissociation. In figure 13, there is a schematic representation of this model for the electrostatic patterning on the silica surface.

4.3. Stöber silica particles

Silica particles with low size dispersity can be prepared by a convenient method proposed by Stöber *et al* [164]. Minor changes in the preparation parameters produce particles in different size ranges and these can be further used to make thin silica films and glasses. Figure 14 shows AFM and KFM micrographs from dry silica particles prepared by this method. KFM images show that the interior of the particles is more negative than their shells and interstitial domains [165], with steep potential gradients at the particle borders. Imaging particles of different average sizes, it is also possible to observe that smaller particles show large differences in electrostatic potential, while larger particles show more uniform core–shell particle potential patterns (figure 14).

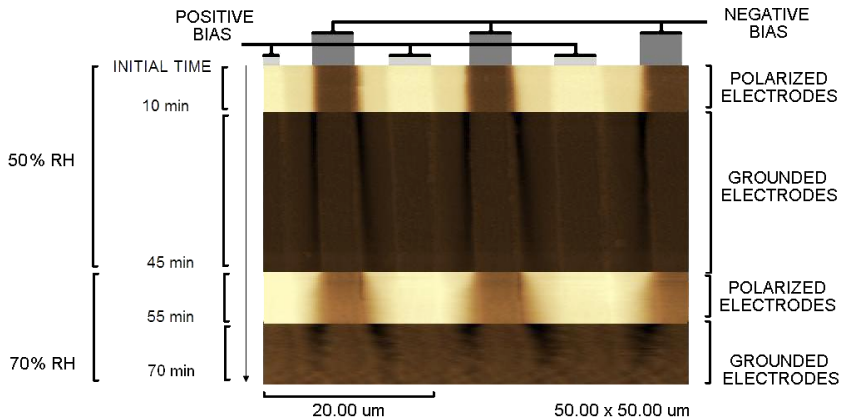

Figure 12. KFM micrograph of a silica-on-wafer thin film partially covered with interdigitated electrodes. Successive changes on electrode polarization, acquisition time and relative humidity were made during image acquisition, as indicated at the sides of the figure. Brighter areas are positive; darker areas are negative.

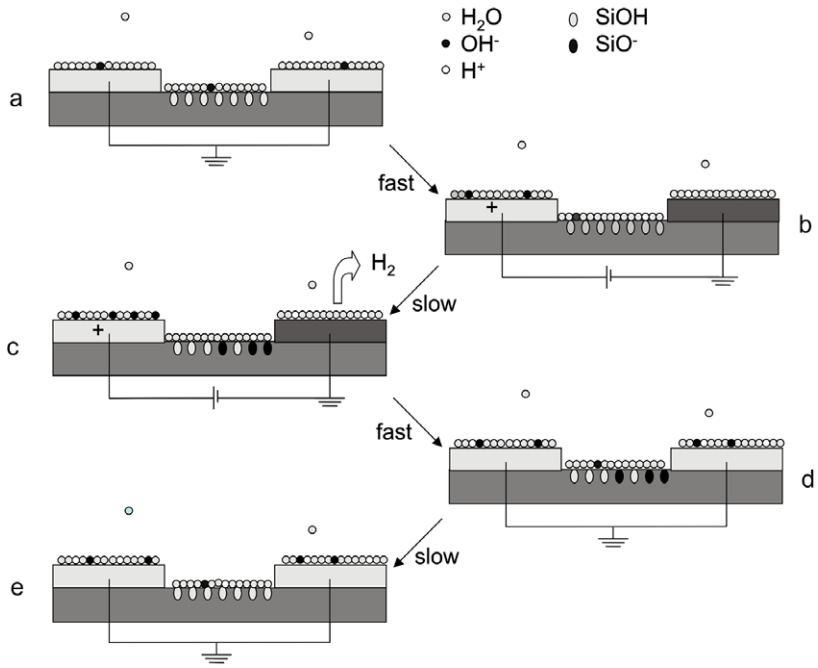

Figure 13. Schematic model for the behaviour of water molecules in the electrodes and silica surface, as well as of the silanol groups on silica: (a) in the initial state, the water film is neutral, at the gas–solid interfaces; (b) when an electrode set is biased, surface ions migrate to electrodes carrying potential of opposite signal; (c) silanol groups are slowly converted to silicate while H^+ ions are discharged at the grounded electrode; (d) when the electrodes are all grounded, ions at the surface film migrate re-forming a neutral water layer; (e) silicate groups bind H^+ ions from water and they are thus neutralized.

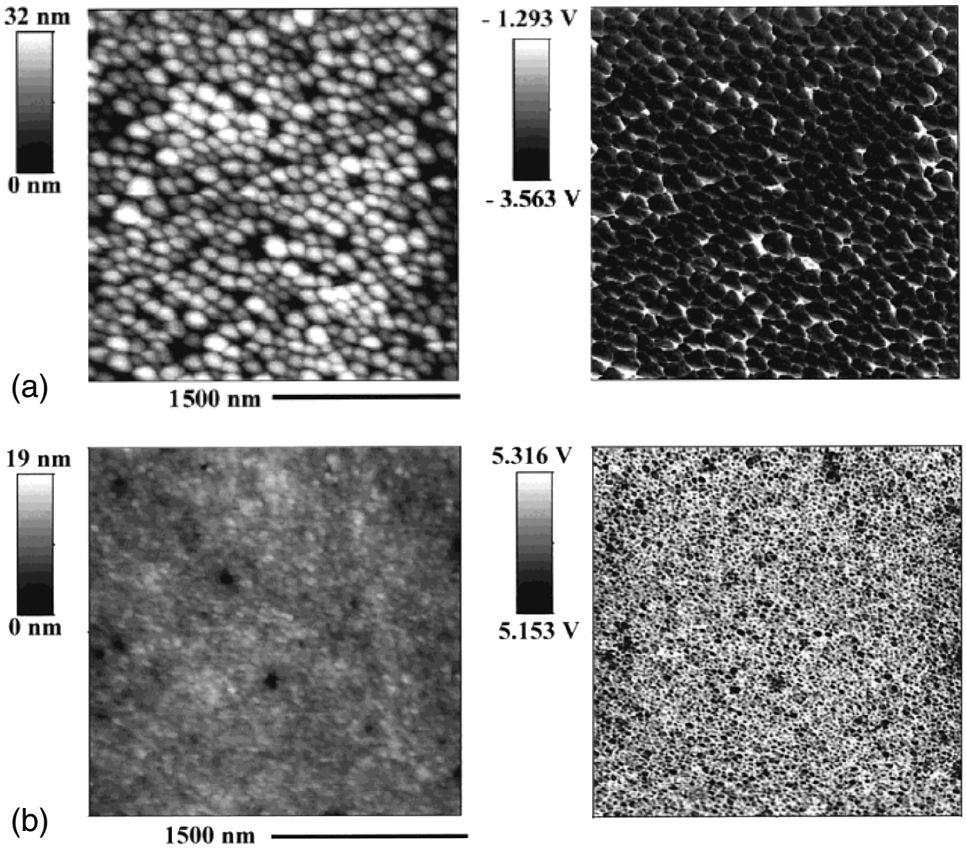

Figure 14. AFM (left) and KFM (right) images of the larger (about 141 nm, top) and smaller (about 36 nm, bottom) Stöber silica particles.

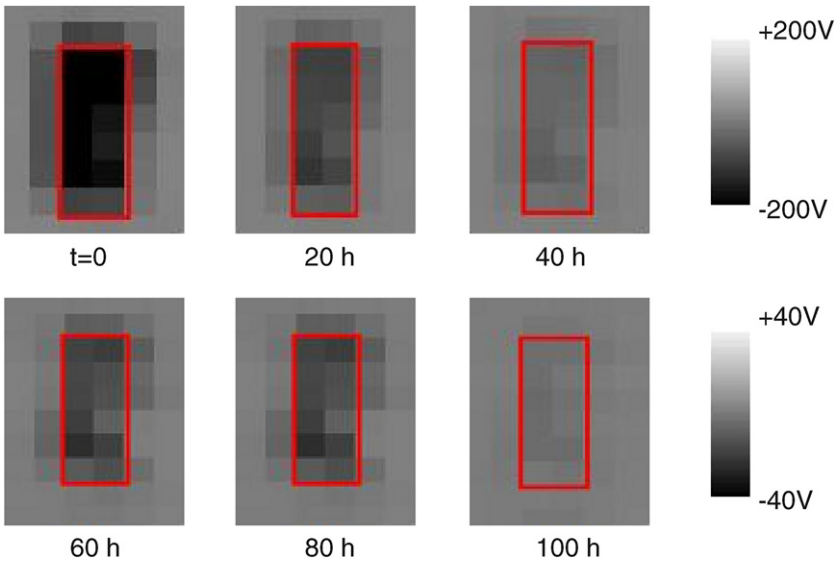

Figure 15. Macroscopic potential maps measured on a polyethylene slab (3 cm × 1 cm) using a Kelvin electrode, as a function of equilibration time. Red rectangles delimit the LDPE sample area.

4.4. Thermoplastics

Typical thermoplastics such as polyethylene, polypropylene and polystyrene are formed by linear or branched chains containing carbon and hydrogen atoms, which should produce only electroneutral structures. Some other species bearing electric charges are expected in thermoplastics due to: (i) contaminants, including catalyst residues; (ii) charged species tribochemically produced during extrusion and other thermomechanical processing; (iii) oxidation and photo-oxidation products due to air and sunlight exposure; and (iv) other high-energy species formed due to background radiation such as cosmic rays. Electroneutrality in any physical medium implies that ionic species carrying opposite charges should occupy neighbouring sites and that they should also move simultaneously [166].

The distribution of electric potentials in thermoplastics observed using KFM was reported for the first time by this group, showing irregular electric patterns on polyethylene and polypropylene surface with high contrast [106]. Topography and electric potential images were simultaneously obtained and a variable degree of correlation is observed between them, giving evidence of the independence of topography and electrical features on the sample.

In recent work by this group (to be published), macroscopic potential measurements on the surface of low density polyethylene (LDPE) slabs (3 cm^2) lying on an aluminium plate showed heterogeneous behaviour between neighbouring areas both concerning the potential distribution in the surface plane and the decay as a function of time. Successive maps of potential distribution on the same polyethylene sample are presented in figure 15.

Polyethylene slabs were carefully washed with NaOH solution and rinsed many times with distilled and deionized water. They were then deposited on the aluminium plate to dry in an oven at 60 °C and potential measurements started right after drying. Potential maps were acquired using a scanning Kelvin electrode of diameter 5 mm, which determines the size of the pixels on the image. The relative humidity was kept at $(60 \pm 2)\%$ and the temperature at (25 ± 2) °C.

Measurements taken just after the samples were corona charged show three distinct areas: (1) a negative potential area (<-200 V in many points) on the polyethylene slab; (2) a bordering area on the aluminium plate with potential predominantly negative and (3) an outer region over the aluminium plate with zero potential. The potential bars are in grey scale and scanning times are between 0 and 100 h.

Polyethylene potential decays with the time and, after 20 h, less negative potential areas can be observed on the slab, forming a heterogeneous pattern. Neighbouring regions showing distinct potential values and the heterogeneous pattern persist for more than 80 h until the potential reaches equilibrium.

Thermoplastics showing large overall electrostatic potentials are not easily imaged in the scanning probe microscope. However, if they are allowed to equilibrate under a defined relative humidity, preferably above 50%, KFM micrographs can be obtained [106].

Thus, thermoplastics show electrified domains in any size range, from a few tens of nanometres to many centimetres and probably also above and below this range.

In the case of thermoplastics, the identity of charges could not yet be established as effectively as in the case of latex or silica particles. This is because sampling for analytical TEM necessarily involves ultramicrotomy and, thus, there is a large possibility for tribochemical charge formation.

4.5. Cellulose

Cellulose is a neutral polymer that may carry some acid–base groups due to oxidation, especially carboxyl and carboxylate groups. In this laboratory it was used to study charge

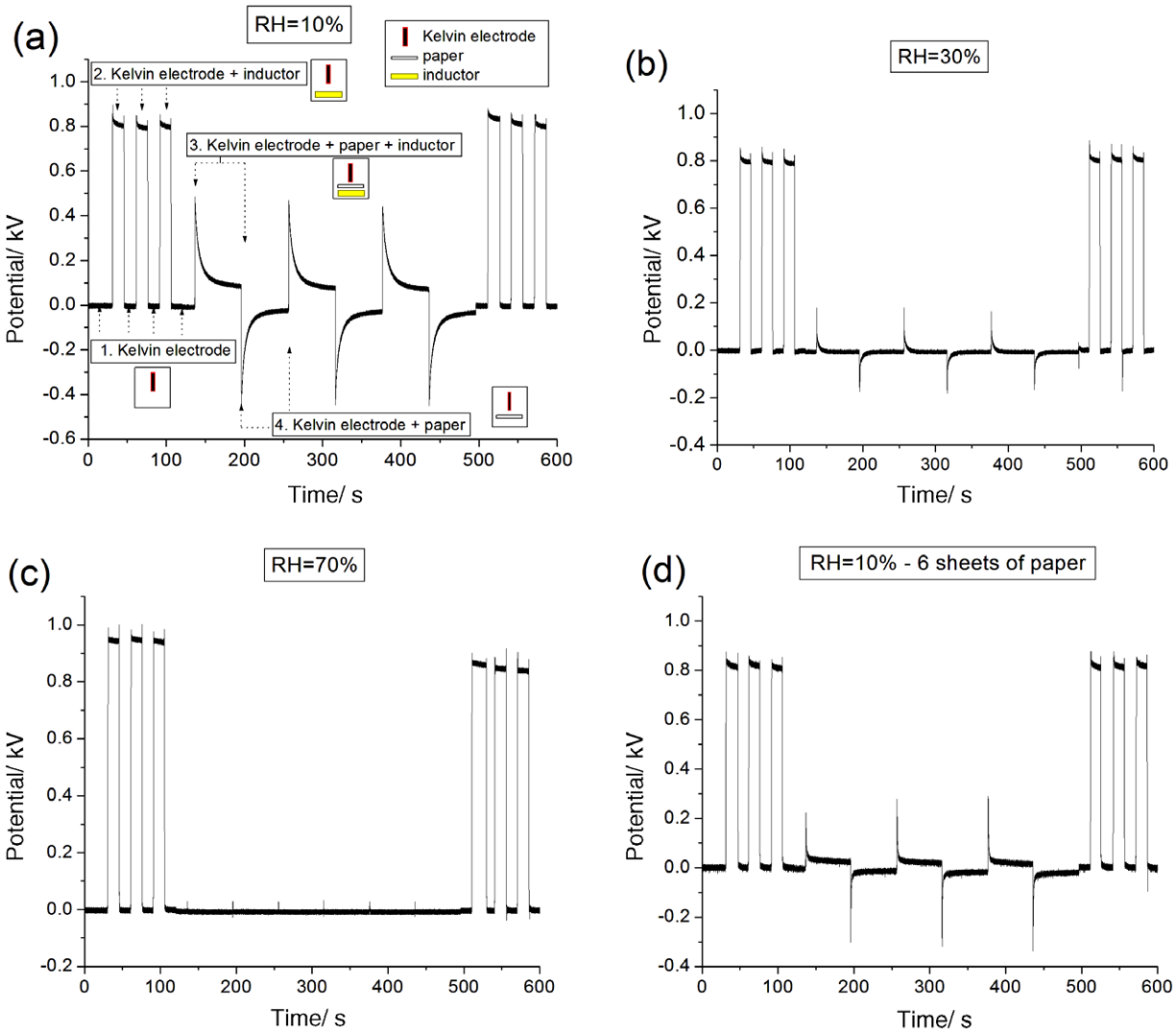

Figure 16. Potential versus time curves for paper under a N_2 atmosphere: (a)–(c) One sheet of paper, RH from 10–70%; (d) six sheets of paper, RH = 10% [27].

induction and dissipation in dielectrics. Electrostatic charge is accumulated on cellulose following the approximation of a charged acrylic sheet. Then it is dissipated when the acrylic inductor is moved away [27]. Electrostatic potential adjacent to cellulose sheets was determined using a Kelvin voltmeter set-up. The paper samples were placed beneath the electrode, and the acrylic inductor was approximated either beneath or above the cellulose sheet, under room temperature and a humidified N_2 atmosphere. The measured potential (V) was recorded as a function of time during the consecutive charging–discharging cycles, as shown in figure 16 for different relative humidity values (10–70%) and numbers of paper sheets.

In figure 16(a), a scheme shows the correlation between potential curve features and the experimental procedure steps: (1) introduction of the Kelvin electrode; (2) introduction of the inductor beneath the electrode; (3) insertion of the paper sheet between the electrode and the inductor (charging step) and (4) removal of the inductor, measuring the induced potential decay (dissipation step).

Under a positive inductor potential, paper acquires excess negative charges, which are lost when the inductor is removed. A symmetrical behaviour was observed for charge build-up and dissipation curves together with a pronounced effect of the relative humidity. Maximum and minimum potentials read when the inductor is introduced or removed change as well as the decay rate constants (k) of the $V \times t$ curves that were fitted according to the $V = V_0 + [Ae^{(-kt)}]$ equation.

Increase in the number of paper sheets or in the relative humidity increases the amount of adsorbed water separating the electrode and the inductor.

These results are explained as follows: atmospheric water adsorbed on the insulator surface acquires excess charges due to the displacement of the water dissociation equilibrium under a non-zero potential. This results in adsorption ion imbalance and in excess concentration of $H(H_2O)_n^+$ or $OH(H_2O)_n^-$ depending on the applied potential. When the acrylic inductor is removed from the vicinity of the cellulose, water ion clusters are desorbed to the atmosphere and the potential on the paper sheet falls back to the initial value.

This model is based on simple and classical concepts which have been extensively applied in colloid and surface science: the existence of ions in the atmosphere, water self-ionization equilibrium, excess local charge formation under a non-zero potential according to the Poisson–Boltzmann equation distribution and adsorption equilibrium. These ideas have not been previously applied to explain electrostatic induction phenomena in insulators, but so far they have been successfully used in the authors' laboratory.

5. Conclusion and perspectives

Electrostatic charging and discharging phenomena are associated with a large number of complex physico-chemical events including some that are very poorly known. We can thus easily understand why they have evaded the theoretical and even phenomenological frameworks that were built for them.

The fundamental question of the identity of the species that account for charge excess in insulators still receives conflicting answers in the literature, but reports evidencing the role of ions are being published in increasingly larger numbers. The complexity of the role of water is now acknowledged, especially as a source of ions, and the introduction of ideas on the atmosphere as a source and sink of ions is giving a new impetus to models based on water ion adsorption, providing detailed and effective explanations for a number of puzzling observations.

Progress along this line depends on a large amount of currently unavailable information. First, the electrochemistry of the air under ambient conditions is not a developed area as opposed to the rather mature state of electrochemistry in plasmas and condensed matter. Electrochemistry at the solid–gas interface is almost exclusively devoted to the study of high-temperature fuel cells within very specific systems. Water is truly ubiquitous: not only does it bind tightly to most solid surfaces, including polymers, but it is also tenaciously soluble in non-polar media such as hydrocarbons, albeit in rather limited amounts.

The situation is further complicated by one simple factor: few excess charges generate large electrostatic potentials. Thus, ion excess concentrations that are not detected using the most sophisticated current tools can account for easily measurable potentials.

Another major new advancement is the recognition of the ubiquity of complex charge patterns, since they have been found in any insulator surface that has been examined so far. This is a major conceptual departure from ideas based on the behaviour of metals and semiconductors that have permeated this field. Analogy to metals led almost every researcher in electrostatics to give greater or lesser attention to the triboelectric series that were established by analogy to the contact potential series in metal–metal junctions. However, metal surfaces are equipotential, other than for changes caused by geometry and by oxide and contaminating layers, while insulators are not at all equipotential.

As a result of conceptual developments, reproducible electrostatic patterns are being obtained in a growing number of systems, showing that the underlying electrification models are more and more adequate.

Control of electrostatic charge and discharge is needed for increased health and safety compliance, especially in relation to powder explosion control.

Tesla devoted his attention to the possibility of collecting atmospheric electricity and using it as a source of power. The USPTO patent database describes many ideas and devices for that purpose but these are currently not even considered as a possibility for alternative power generation. On the other hand, atmospheric electricity continues to take a heavy toll in human lives every year. Knowing 'what' atmospheric electricity is, i.e. which are the charge bearing species and the mechanisms for their formation and dissipation, will certainly help us to handle it better than we can do now. Moreover, since atmospheric electricity is intimately connected to thunderstorms, its control may open the way for the control of currently disastrous storms followed by devastating floods throughout the world.

Closer to the ground, clear recognition of the interplay between water (at interfaces or bulk phase) and surrounding electrostatic fields can lead to progress in many areas, from electric phenomena in low-conductivity liquids to adsorption and nucleation, including fascinating biological problems that are currently more or less overlooked.

To sum up, we are now in at a moment of acceleration of knowledge in an old and problematic area, even though some may consider it 'well established'. An important new actor in this play is water, as pervasive as electrostatic phenomena themselves. We can then expect further faster progress both concerning our understanding of natural phenomena and a large number of applications and conceivable new technologies.

Acknowledgments

CAR is a FAPESP post-doctoral fellow and RFG is a CNPq predoctoral fellow. FG acknowledges support from CNPq and FAPESP (Millennium Institute Programme and National Institutes for Science and Technology Programme).

References

[1] Maxwell J C 1892 *A Treatise on Electricity and Magnetism* 3rd edn, vol 1 (New York: Dover)
[2] Schein L B 1992 *Electrophotography and Development Physics* (Berlin: Springer)
[3] Gerhard-Mulhaupt R and Joseph M C 1999 *Electrets* 3rd edn (California: Laplacian press)
[4] Sessler G M 2001 *J. Electrostat.* **51/52** 137
[5] Kressmann R, Sessler G M and Günther P 1996 *IEEE Trans. Dielectr. Electr. Insul.* **3** 607
[6] Taylor M D and Seeker P E 1994 *Industrial Electrostatics: Fundamentals and Measurements* (Stevenage: Research Studies Press)
[7] Frenot A and Chronakis I S 2003 *Curr. Opin. Colloid Interface Sci.* **8** 64–75
[8] Moshkin A A and Moshkina S A 1997 *J. Electrostat.* **40/41** 681
[9] Lowell J and Rose-Innes A C 1980 *Adv. Phys.* **29** 947

[10] Schein L B 2007 *Science* **316** 1572
[11] Bailey A G 2001 *J. Electrostat.* **51/52** 82
[12] Giles M R 2003 *Org. Process Res. Dev.* **7** 1048
[13] Material available from http://www.esdjournal.com/
[14] Taillet J 2003 *Powder Technol.* **135/136** 201
[15] Rowley G 2001 *Int. J. Pharm.* **227** 47
[16] Material available from http://www.esda.org/
[17] Schein L B, La Ha M and Marshall G 1991 *J. Appl. Phys.* **69** 6817
[18] Castle G S P 1997 *J. Electrostat.* **40/41** 13
[19] Teyssedre G and Laurent C 2005 *IEEE Trans. Dielectr. Electr. Insul.* **12** 857
[20] Montanari G C and Morshuis P H F 2005 *IEEE Trans. Dielectr. Electr. Insul.* **12** 754
[21] Castle G S P and Schein L B 1995 *J. Electrostat.* **36** 165
[22] Chen G, Tanaka Y, Takada T and Zhong L 2004 *IEEE Trans. Dielectr. Electr. Insul.* **11** 113
[23] McCarty L S and Whitesides G M 2008 *Angew. Chem. Int. Edn* **47** 2188
[24] Liu C and Bard A J 2008 *Nat. Mater.* **7** 505
[25] Perrin C, Griseri V, Inguimbert C and Laurent C 2008 *J. Phys. D: Appl. Phys.* **41** 205417
[26] Griffiths D J 1999 *Introduction to Electrodynamics* 3rd edn (Upper Saddle River, NJ: Prentice-Hall)
[27] Soares L C, Bertazzo S, Burgo T A L, Baldim V and Galembeck F 2008 *J. Braz. Chem. Soc.* **19** 277
[28] Yovcheva T A, Mekishev G A and Marinov A T 2004 *J. Phys.: Condens. Matter* **16** 455
[29] Hogue M D, Buhler C R, Calle C I, Matsuyama T, Luo W and Groop E E 2004 *J. Electrostat.* **61** 259
[30] Folan L M, Arnold S, O'Keeffe T R, Spock D E, Schein L B and Diaz A F 1990 *J. Electrostat.* **25** 155
[31] Németh E, Albrecht V, Schubert G and Simon F 2003 *J. Electrostat.* **58** 3
[32] Reichardt C 1994 *Chem. Rev.* **94** 2319
[33] El Seoud O A, Fidale L C, Ruiz N, D'Almeida M L and Frollini E 2008 *Cellulose* **15** 371
[34] Spange S, Reuter A and Ludba D 1999 *Langmuir* **15** 2103
[35] Bauer S and Bauer-Gogonea S 2003 *IEEE Trans. Dielectr. Electr. Insul.* **10** 883
[36] Collins R E 1980 *J. Appl. Phys.* **51** 2973
[37] Cernomorcenco A and Notingher P 2008 *Appl. Phys. Lett.* **93** 192903
[38] Palowski T, Fleming R J and Lang S B 2006 *IEEE Trans. Dielectr. Electr. Insul.* **13** 1023
[39] Afanasjev V P, Petrov A A, Pronin I P, Tarakanov E A, Ju Kaptelov E and Graul J 2001 *J. Phys.: Condens. Matter* **13** 8755
[40] Takada T 1999 *IEEE Trans. Dielectr. Electr. Insul.* **6** 519
[41] Holé S, Sylvestre A, Gallot-Lavallée O, Guillermin C, Rain P and Rowe S 2006 *J. Phys. D: Appl. Phys.* **39** 950
[42] Paris O, Lewiner J, Ditchi T, Holé S and Alquié C 2000 *IEEE Trans. Dielectr. Electr. Insul.* **7** 556
[43] Mizutani T 1994 *IEEE Trans. Dielectr. Electr. Insul.* **1** 923
[44] Maeno T, Futami T, Kushibe H, Takada T and Cooke C M 1998 *IEEE Trans. Electr. Insul.* **23** 433
[45] Migliori A and Thompson J D 1980 *J. Appl. Phys.* **51** 479
[46] Rozno A G and Gromov V V 1986 *IEEE Trans. Electr. Insul.* **21** 417
[47] Gégot F, Callegari Th, Aillerie M and Boeuf J P 2008 *J. Phys. D: Appl. Phys.* **41** 135204
[48] Okubo H, Wakamatsu M, Inoue N, Kato K and Koide H 2003 *IEEE Trans. Dielectr. Electr. Insul.* **10** 956
[49] Martin B and Kliem H 2008 *IEEE Trans. Dielectr. Electr. Insul.* **15** 560
[50] Nonnenmacher M, O' Boyle M P and Wickramasinghe H K 1991 *Appl. Phys. Lett.* **58** 2921
[51] Jacobs H O, Knapp H F and Stemmer A 1999 *Rev. Sci. Instrum.* **70** 1756
[52] Liscio A, Palermo V, Müllen K and Samorì P 2008 *J. Phys. Chem.* C **112** 17368
[53] Cunningham S 1996 *Appl. Phys. Lett.* **69** 3605
[54] Lambert J, Guthmann C and Saint-Jean M 2003 *J. Appl. Phys.* **93** 5369
[55] Marchi F, Dianoux R, Smilde H J H, Mur P, Comin F and Chevrier J 2008 *J. Electrostat.* **66** 538
[56] Gong H and Ong C K 1997 *J. Phys.: Condens. Matter* **9** 1631
[57] Bigarré J, Attard C, Hourquebie P and Matallana J 2001 *IEEE Trans. Dielectr. Electr. Insul.* **8** 942
[58] Gerhard-Mulhaupt R, Künstler W, Eberle G, Eisenmenger W and Yang G 1998 *Space Charge in Solid Dielectric* (UK: The Dielectrics Society) p 123
[59] Bloss P, DeReggi A S, Yang G M, Sessler G M and Schafer H 2000 *J. Phys. D: Appl. Phys.* **33** 430
[60] Bloss P, Steffen M, Schaffer H, Yang G M and Sessler G M 1997 *J. Phys. D: Appl. Phys.* **30** 1668
[61] Alquié C, Dreyfus G and Lewiner J 1981 *Phys. Rev. Lett.* **47** 1483
[62] Takada T, Miyake H and Tanaka Y 2006 *IEEE Trans. Plasma Sci.* **34** 2176
[63] Mellinger A, Flores-Suárez R, Singh R, Wegener M, Wirges W, Gerhard R and Lang S B 2008 *Int. J. Thermophys.* **29** 2046
[64] Lang S B and Das-Gupta D K 1986 *J. Appl. Phys.* **59** 2151
[65] Wubbenhorst M, Hornsby J, Stachen M, Das-Gupta D K, Bulinski A and Bamji S 1998 *IEEE Trans. Dielectr. Electr. Insul.* **5** 9
[66] Marin-Franch P, Tunnicliffe D L and Das-Gupta D K 2001 *Mater. Res. Innov.* **4** 334
[67] Fleming R J, Pawlowski T, Ammala A, Casey P S and Lawrence K A 2005 *IEEE Trans. Dielectr. Electr. Insul.* **4** 745
[68] Fleming R J, Ammala A, Casey P S and Lang S B 2008 *IEEE Trans. Dielectr. Electr. Insul.* **15** 118
[69] Cecelja F, Bordovsky M and Balachandran W 2002 *IEEE Trans. Instrum. Meas.* **51** 282
[70] Zahn M, Hikita M, Wirght K A, Cooke C M and Brennan J 1987 *IEEE Trans. Electr. Insul.* **22** 181
[71] Ahmed N H and Srinivas N N 1997 *IEEE Trans. Dielectr. Electr. Insul.* **4** 644
[72] Cardoso A H, Leite C A P and Galembeck F 1998 *Langmuir* **14** 3187
[73] Cardoso A H, Leite C A P and Galembeck F 1999 *Langmuir* **15** 4447
[74] Egerton R F 1986 *Electron Energy-Loss Spectroscopy in the Electron Microscope* (New York: Plenum)
[75] Botton G 2007 Analytical electron microscopy *Science of Microscopy* ed P W Hawkes and J C H Spence (New York: Springer) p 273
[76] Amalvy J I, Percy M J, Armes S P, Leite C A P and Galembeck F 2005 *Langmuir* **21** 1175
[77] Ottensmeyer F P 1984 *J. Ultrastruct. Res.* **88** 121
[78] Shuman H, Chang C F and Somlyo A P 1986 *Ultramicroscopy* **19** 121
[79] Linares E M, Leite C A P, Valadares L F, Silva C A, Rezende C A and Galembeck F 2009 *Anal. Chem.* **81** 2317
[80] Bulliard C, Allan M and Leach S 1993 *Chem. Phys. Lett.* **209** 434
[81] Leapman R D 2003 *J. Microsc.* **210** 5
[82] Leite C A P and Galembeck F 2001 *J. Colloid Interface Sci.* **235** 4
[83] Valadares L F, Bragança F D C, Silva C A, Leite C A P and Galembeck F 2007 *J. Colloid Interface Sci.* **309** 140
[84] Galembeck F, Costa C A R, Galembeck A and Silva M C V M 2001 *An. Acad. Bras. Cienc.* **73** 495
[85] Thomson W 1898 *Phil. Mag.* **46** 82
[86] Zisman W A 1932 *Rev. Sci. Instrum.* **3** 367

[87] Galembeck F and Costa C A R 2006 *Encyclopedia of Surface and Colloid Science* (New York: Dekker) p 1874
[88] Cheran L E and Thompson M 2004 *Analyst* **129** 406
[89] Yee S, Oriani R A and Stratmann M 1991 *J. Electrochem. Soc.* **138** 55
[90] Thompson M, Cheran L E, Zhang M, Chacko M, Huo H and Sadeghi S 2005 *Biosens. Bioelectron.* **20** 1471
[91] Jacobs H O, Knapp H F, Müller S and Stemmer A 1997 *Ultramicroscopy* **69** 39
[92] Mizsei J 2002 *Solid-State Electron.* **46** 235
[93] Jankov I R, Szente R N, Goldman I D, Carreno M N P, Valle M A, Behar M, Costa C A R, Galembeck F and Landers R 2005 *Surf. Coat. Technol.* **200** 254
[94] Li W and Li D Y 2005 *J. Chem. Phys.* **122** 64708
[95] Jacobs H O, Leuchtmann P, Homan O J and Stemmer A 1998 *J. Appl. Phys.* **84** 1168
[96] Mizsei J 1998 *Sensors Actuators* B **48** 300
[97] Cheran L E, McGovern M E and Thompson M 2000 *Faraday Discuss.* **116** 23
[98] McCarty L S, Winkleman A and Whitesides G M 2007 *Angew. Chem. Int. Edn* **46** 206
[99] Jacobs H O and Whitesides G M 2001 *Science* **291** 1763
[100] McCarty L S, Winkleman A and Whitesides G M 2007 *J. Am. Chem. Soc.* **129** 4075
[101] Barry C R, Gu J and Jacobs H O 2005 *Nano Lett.* **5** 2078
[102] Stemmer A, Ziegler D, Seemann L, Rychen J and Naujoks N 2008 *J. Phys.: Conf. Ser.* **142** 012048
[103] He T, Ding H, Peor N, Naama P, Lu M, Corley D A, Chen B, Ofir Y, Gao Y, Yitzchaik S and Tour J M 2008 *J. Am. Chem. Soc.* **130** 1699
[104] Taylor D M, Morris D and Cambridge J A 2004 *Appl. Phys. Lett.* **85** 5266
[105] Keslarek A J, Costa C A R and Galembeck F 2001 *Langmuir* **17** 7886
[106] Galembeck A, Costa C A R, Silva M C V M, Souza E F and Galembeck F 2001 *Polymer* **42** 4845
[107] Sahli S, Bellel A, Ziari Z, Kahlouche A and Segui Y 2003 *J. Electrostat.* **57** 169
[108] Braga M, Costa C A R, Leite C A P and Galembeck F 2001 *J. Phys. Chem.* B **105** 3005
[109] Gouveia R F, Costa C A R and Galembeck F 2005 *J. Phys. Chem.* B **109** 4631
[110] Gouveia R F, Costa C A R and Galembeck F 2008 *J. Phys. Chem.* C **112** 17193
[111] Dongmo H, Carlotti J F, Bruguier G, Guasch C, Bonnet J and Gasiot J 2003 *Appl. Surf. Sci.* **212/213** 607
[112] Ben Nasr T, Kamoun N and Guasch C 2006 *Mater. Chem. Phys.* **96** 84
[113] Prasse T, Ivankov A, Sandler J, Schulter K and Baughofer W 2001 *J. Appl. Polym. Sci.* **82** 3381
[114] Cheran L E, Cheung S, Wang X and Thompson M 2008 *Electrochim. Acta* **53** 6690
[115] Kikukawa A, Hosaka S and Imura R 1995 *Appl. Phys. Lett.* **66** 3510
[116] Weaver J M R and Abraham D W 1991 *J. Vac. Sci. Technol.* B **9** 1559
[117] Gouveia R F and Galembeck F 2009 submitted
[118] Rigden J S 1996 *Macmillan Encyclopedia of Physics* (New York: Macmillan)
[119] Derjaguin B V and Smilga V P 1967 *J. Appl. Phys.* **38** 4609
[120] Derjaguin B V, Krotova N A and Smilga V P 1978 *Adhesion of Solids* (New York: Consultants Bureau)
[121] Wu S 1982 *Polymer Interface and Adhesion* (New York: Dekker)
[122] Valadares L F, Leite C A P and Galembeck F 2006 *Polymer* **47** 672
[123] Boss S L B and Caluzi J J 2007 *Rev. Bras. Ens. Fis.* **29** 635
[124] Diaz A F and Felix-Navarro R M 2004 *J. Electrostat.* **62** 277
[125] Heinicke G 1984 *Tribochemistry* (Berlin: Carl Hanser)
[126] Camara C G, Escobar J V, Hird J R and Putterman S J 2008 *Nature* **455** 1089
[127] Dole M 1973 *The Radiation Chemistry of Macromolecules* (New York: Academic)
[128] de Barros R A and Azevedo W M 2008 *Synth. Met.* **158** 922
[129] Rocha R M, Moura E A B, Bressiani A H A and Bressiani J C 2008 *J. Mater. Sci.* **43** 4466
[130] Son C and Ziaie B 2006 *IEEE Electron Device Lett.* **27** 884
[131] Parada M A, Minamisawa R A, Moreira M V, de Almeida A, Muntele I and Ila D 2007 *Surf. Coat. Technol.* **201** 8246
[132] Das-Gupta D K and Schmidt W F 1995 *IEEE Trans. Compon. Packag. Manufact. Technol.* A **18** 266
[133] Das-Gupta D K 1992 *IEEE Trans. Electr. Insul.* **27** 908
[134] Kotrappa P 2005 *Health Phys.* **89** 164
[135] Giacometti J A and Oliveira O N Jr 1992 *IEEE Trans. Electr. Insul.* **27** 924
[136] Bakhoum S F W and Agnes G R 2005 *Anal. Chem.* **77** 3189
[137] Eberlin L S, Xia Y, Chen H and Cooks R G 2008 *J. Am. Soc. Mass Spectrom.* **19** 1897
[138] Waltman M J, Dwivedi P, Hill H H, Blanchard W C and Ewing R G 2008 *Talanta* **77** 249
[139] Reagan M A, Kashyn D, Juhl S, Vaia R A and Lyuksyutov S F 2008 *Appl. Phys. Lett.* **93** 033109
[140] Ressier L and Le Nader V 2008 *Nanotechnology* **19** 135301
[141] Diaz A F and Fenzel-Alexander D 1993 *Langmuir* **9** 1009
[142] Diaz A F 1998 *J. Adhes.* **67** 111
[143] Law K Y, Tarnawskyj I W and Salamida D 1998 *J. Imaging Sci. Technol.* **42** 465
[144] Medley J A 1953 *Nature* **171** 1077
[145] Diaz A F, Wollmann D and Dreblow D 1991 *Chem. Mater.* **3** 997
[146] Mizes H A, Conwell E M and Salamida D P 1990 *Appl. Phys. Lett.* **56** 1597
[147] Law K Y, Tarnawskyj I W, Salamida D and Debies T 1995 *Chem. Mater.* **7** 2090
[148] Schröndiger E 1910 *PhD Thesis* University of Vienna, Vienna
[149] Seaver E 2005 *J. Electrostat.* **63** 203–22
[150] Turov V V and Mironyuk I F 1998 *Colloids Surf.* A **134** 257
[151] Patton S T, Cowan W D, Eapen K C and Zabinski J S 2000 *Tribol. Lett.* **9** 199
[152] Healy T W and Fuerstenau D W 2007 *J. Colloid Interface Sci.* **309** 181
[153] Huertas M L and Fontan J 1975 *Atmos. Environ.* **9** 1018
[154] Vonnegut B 1994 *Bull. Am. Meteorol. Soc.* **75** 53
[155] Hunter R J 1981 *Zeta Potential in Colloid Science Principles and Applications* (London: Academic)
[156] Banic C M and Iribarne J V 1985 *J. Chem. Phys.* **83** 6432
[157] Ovchinnikova K and Pollack G H 2009 *Langmuir* **25** 542
[158] Lee L T, Silva M C V and Galembeck F 2003 *Langmuir* **19** 6717
[159] Lee L T, Leite C A P and Galembeck F 2004 *Langmuir* **20** 4430
[160] Cardoso A H, Leite C A P, Zaniquelli M E D and Galembeck F 1998 *Colloids Surf.* A **144** 207
[161] Braga M, Costa C A R, Leite C A P and Galembeck F 2001 *J. Phys. Chem.* B **105** 3005
[162] Teixeira-Neto E and Galembeck F 2002 *Colloids Surf.* A **207** 147
[163] Santos J P, Pascale C, Wong K and Galembeck F 2004 *Langmuir* **20** 10576
[164] Stöber W, Fink A and Bohn E 1968 *J. Colloid Interface Sci.* **26** 62
[165] Costa C A R, Leite C A P, Souza E F and Galembeck F 2001 *Langmuir* **17** 189
[166] Wu K, Iedema M J and Cowin J P 1999 *Science* **286** 2482